(Received 8 September 2024, Accepted 4 October 2024, Scheduled 13 October 2024)

A Miniaturized Antipodal Vivaldi Antenna for High-Power Design in X-Band

Liangliang Zhao[1,*], Aidong Li[1], Chuwei Li[2], Yongmao Wang[1], Mingxuan Zheng[3], Dengyang Song[1], Chenlu Liu[1], Yongtao Liang[1], Huiling Zhao[1], Chufeng Hu[4], and Tao Ma[5]

[1]*School of Electronics and Information, Northwestern Polytechnic University, Xi'an, China*
[2]*China Academy of Space Technology (CAST), Beijing, China*
[3]*System Engineering Division, Xi'an Electronic Engineering Research Institute, Xi'an, China*
[4]*Science and Technology on UAV Laboratory, Northwestern Polytechnic University, Xi'an, China*
[5]*The 43rd Research Institute of CETC, Hefei, China*

ABSTRACT: A compact antipodal Vivaldi antenna (AVA) integrated with circularly shaped loads and some elliptic slits etched in tapered slots is proposed in this paper. First, the elliptic slits etched in two tapered slots are employed for wideband application in X-band. Then, the value of max power capacity increasing from 0.47 MW to 0.82 MW is mainly due to two circularly shaped loads. Moreover, the size of the antenna is decreased to $0.44\lambda_{\text{middle}} \times 0.42\lambda_{\text{middle}}$. The configuration is measured to confirm the simulated results. Based on these, a novel antipodal Vivaldi antenna with compact size is successfully designed and applied in high-power field at X-band.

1. INTRODUCTION

With the rapid development of ultra-wideband (UWB) antenna and high-power equipment, high-power planner phase array with UWB antenna units is extensively applied in various radar technologies and communication systems [1–6]. Recently, some investigations of high-power antennas are depicted [7–15]. Generally, high-power antennas cover various categories involving horn antenna [7], mode-transducing antenna [8–10], Vlasov antenna [11, 12], and combined mode convertor with conventional antenna [13]. It is observed that above designs show great performances in high-power fields, and the current antenna must meet the foot space, light weight, and UWB performances simultaneously for the application in Unmanned Aerial Vehicle (UAV) relevant domains.

Gibson proposed a Vivaldi antenna in 1979 [16], which has natural wide impedance bandwidth, relatively lower profile and simple structure. Then, Gazit presented an antipodal Vivaldi antenna in 1988 to further broaden the bandwidth [17]. Next, numerous Vivaldi antennas were proposed to provide better radiation characteristics [18–25], such as a wideband antipodal Vivaldi antenna with tapered slot edge modification which extended the low cut-off frequency to 2.4 GHz from the original 3.3 GHz, whereas the dimension of the antenna is set to $1.33\lambda_{\text{middle}} \times 1.66\lambda_{\text{middle}}$, which is relatively large [18]. By adopting additional regular slot edges, the operating frequency in low band is reduced by 9% [19]. At the same time, configuration of the loaded lens and choke slot edges also enhance the antenna gain. Nevertheless, the antenna with size of $3.91\lambda_{\text{middle}} \times 2.94\lambda_{\text{middle}}$ needs to be further miniaturized. The radiating fins are employed to increase the electrical length thereby lowing the operating bandwidth from 5.2 GHz to 3.7 GHz [20]. The structure achieves 28.8% size reduction with a dimension of $1.52\lambda_{\text{middle}} \times 1.30\lambda_{\text{middle}}$. A new antipodal Vivaldi antenna with a nature fern fractal leaf structure is implemented [21], which makes the lower operating bandwidth of the antenna reduce by 19% compared to the previous iteration. Although the modification of the structure can get more stable radiation characteristics, the prototype could enhance the fabrication costs. A novel W-band surface micromachine tapered with coplanar waveguide and substrate-integrated waveguide is employed for high gain characteristics [22]. The relative bandwidth of the antenna is 37.8%, which needs to be improved. Introducing substrate-integrated waveguide and coplanar waveguide structure can add the complexity of fabrication. A UWB antipodal Vivaldi antenna is composed of a stepped-shaped metamaterial inspired structure and an elliptical-shape director to increase the gain at the high frequencies [23], and the antenna has a broader impedance bandwidth of 186% with a reflection coefficient of lower than -12 dB, and the high gain changes from 4.9 to 14.6 dBi. However, the size of $0.6\lambda_{\text{middle}} \times 1.3\lambda_{\text{middle}}$ requires optimization. Furthermore, a miniaturized and high-gain antipodal Vivaldi antenna with directors is proposed in [24]. By loading some different directors above the radiator, a high-gain Vivaldi antenna for the application in millimeter-wave is realized, whereas the profile of λ_{middle} has potential to optimize. A compact Vivaldi antenna design for breast cancer diagnosis is presented [25]. A specific absorption rate (SAR) value of 0.997 W/kg meets the safety standards, and it offers a wide fractional bandwidth of 143%, which expands the application of Vivaldi antenna.

In this work, a novel antipodal Vivaldi antenna for the application in high-power at X-band is proposed. It consists of

* Corresponding author: Liangliang Zhao (zll18@mail.nwpu.edu.cn).

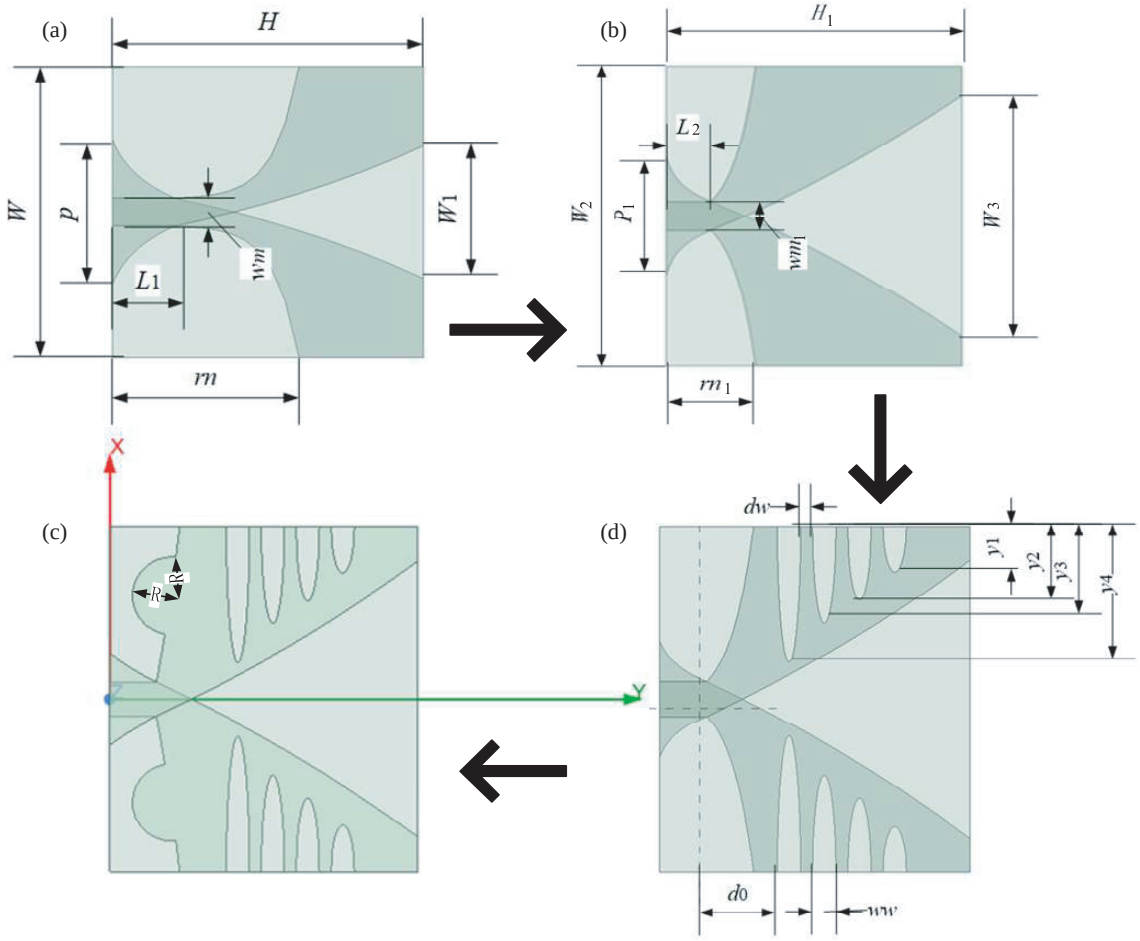

FIGURE 1. Evolution of the proposed configuration. (a) Original AVA. (b) Miniaturized AVA. (c) Modified AVA with some elliptic slits. (d) Modified AVA with some elliptic slits and two circularly shaped loads for high-power designing.

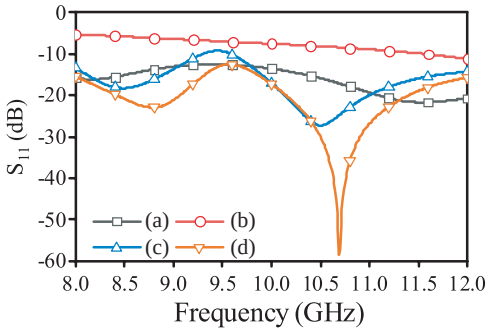

FIGURE 2. Simulated S_{11} of different AVAs.

several elliptic slits etched in several tapered slots for realizing better impedance performances in X-band and circularly shaped loads employed to increase the power capacity. This paper is organized as follows. The antenna design is presented in Section 2. Section 3 depicts simulation and measurement results, and the conclusion is given in Section 4.

2. DESIGN OF PORTABLE SOLAR TELESCOPE

The architecture, evolution, and development of the suggested antenna are detailed in in Fig. 1 and Table 1. At the same time, the simulated S_{11} variation with frequency of AVAs (a) to (d) are shown in Fig. 2. It can be seen that antenna (a) is the initial AVA with an exponentially tapered slot, which is fed by a 50 Ω feedline.

As observed, although the original AVA has a great reflection coefficient, it does not meet the requirement of miniaturization. In AVA (b), the overall dimension decreases from $24 \times 24\,\text{mm}^2$ ($0.80\lambda_{\text{middle}} \times 0.80\lambda_{\text{middle}}$) to $12.6 \times 13.2\,\text{mm}^2$ ($0.44\lambda_{\text{middle}} \times 0.42\lambda_{\text{middle}}$), and the dimension of AVA (b) is far lower than traditional Vivaldi antenna, intending to achieve miniaturized size. Unfortunately, the impedance characteristics of the miniaturized AVA are rapidly deteriorated, which still need to be improved. Next, some notches and gaps are commonly employed in AVA (c) to lengthen the current path, leading to the improvement of impedance characteristics. After adding the elliptic slits etched in the tapered slot in miniaturized AVA, the impedance mismatch will appear around 9.5 GHz. To circumvent the issue, the AVA (d) adopts two circle loads to further add the current path and increase the radiation area, and the proposed antenna achieves better impedance performances in X-band. More significantly, the power capacity is also improved obviously due to the introduction of two circle loads. Ultimately, the final design is achieved.

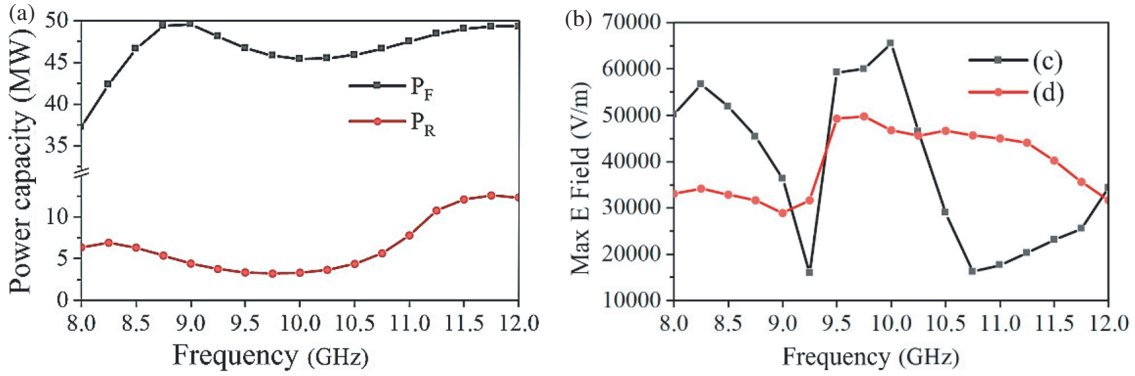

FIGURE 3. Simulated max E field of different AVAs.

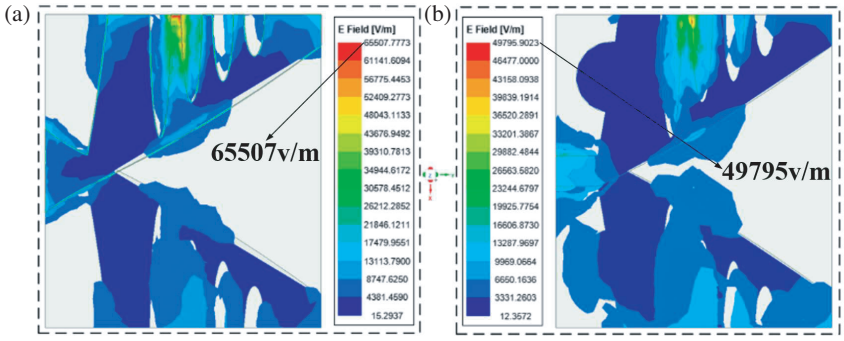

FIGURE 4. Electric-field distributions of different AVAs at 10 GHz. (a) AVA. (b) AVA.

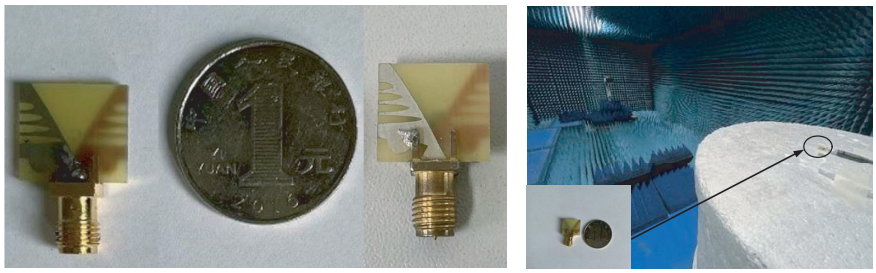

FIGURE 5. Fabricated antenna and its experiment scene.

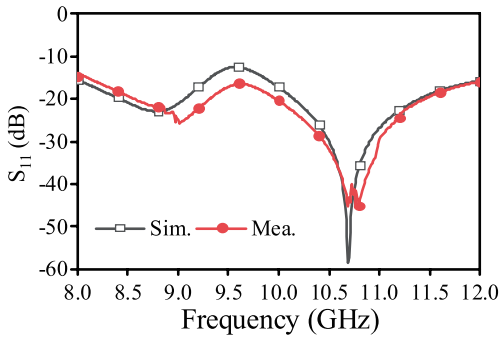

FIGURE 6. Measured and simulated results of proposed AVA.

Meanwhile, high-power design is a significant requirement in military communication field, and it is worthy of investment. In formula (1), E_d is the breakdown field of the substrate, h the thickness of the substrate, Z_0 the characteristic impedance of the microstrip feedline, ρ the voltage standing wave ratio, P_F the power capacity of the feedline portion, and finally P_R represents the power capacity of the radiation part. Because the max E field of AVAs (a) and (b) are lower than 25000 V/m, and the breakdown power of the FR4 is around 37.3 MW, the power capacity of the AVA (a) in the radiation part is around 3.23 MW. Fig. 3(a) plots the power capacity of P_F and P_R, respectively. It is apparent that the value of P_R is less than P_F, which leads to the breakdown of radiation structure easily. Combined with Figs. 3(b), 4, and Equation (2), AVA (d) obtains lower electric filed than AVA (c), which leads to that AVA (d) achieves higher power capacity.

$$P_F = \frac{E_d^2 h^2}{\rho Z_0} \tag{1}$$

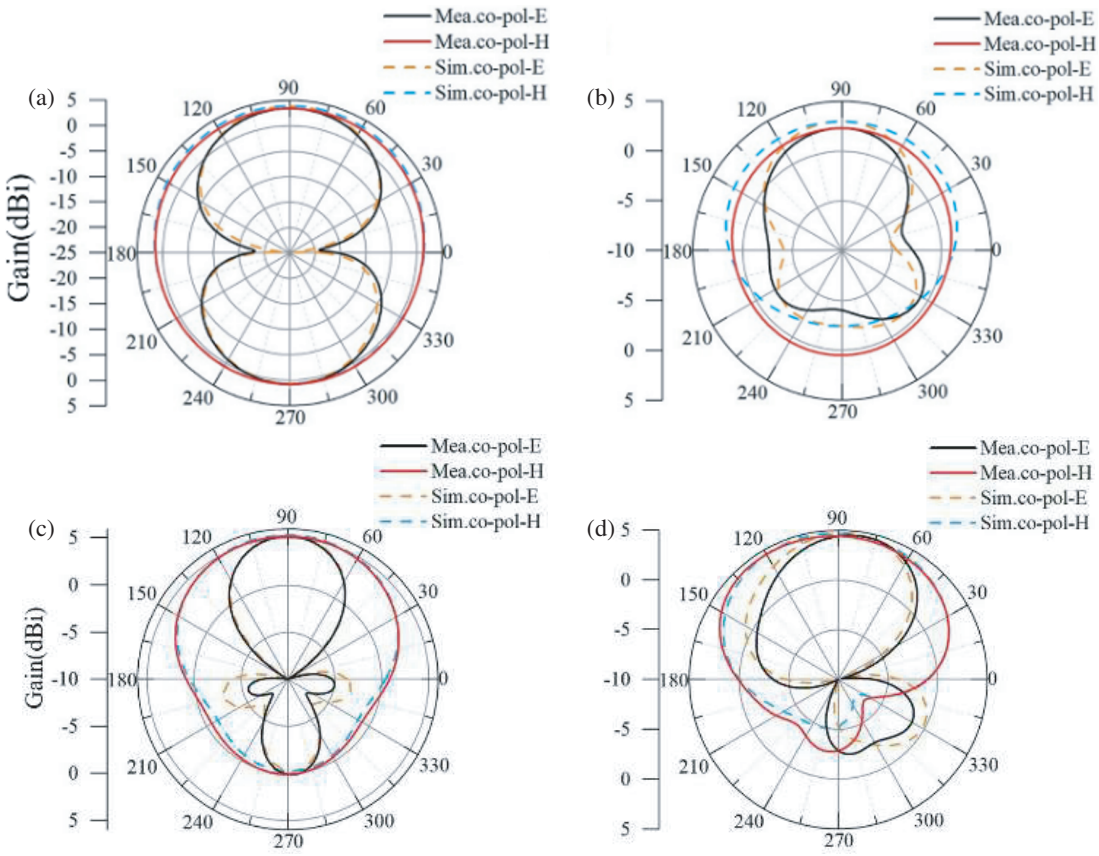

FIGURE 7. Measured and simulated radiation patterns of proposed AVA. (a) 8 GHz. (b) 9 GHz. (c) 10 GHz. (d) 12 GHz.

TABLE 1. Details of AVA.

Parameter	H	W	W_1	P	L1	wm	rn	H1	W_2	W_3	P_1
Value (mm)	24	24	11	12	5	2.3	15	12.6	13.2	10.6	4
Parameter	L_2	wm1	rn1	d_0	ww	dw	y_1	y_2	y_3	y_4	R
Value (mm)	2	1.5	3.7	4	1	0.5	2	3.2	4.2	5.4	1.7

$$P_R = \left(\frac{E_d}{E_{\max}}\right)^2 P_0 \tag{2}$$

The dimension of the UWB antenna is shown in Fig. 1, and it is fabricated on a $46 \times 37\ \text{mm}^2$ FR4 dielectric substrate with a relative dielectric constant of 4.4 and a thickness of 0.7 mm. A tapered microstrip feedline is employed for exciting the identical hexagon-shaped patch. Then, by adding T-shaped structures and etching T-shaped slots, the mutual coupling is suppressed to attain a high isolation and broaden the operational bandwidth. By etching circle slots and several U-shaped slots, four frequently-used stopbands are achieved, respectively. It is worth noting that the evolution of the designed dual-port monopole multiple-input multiple-output (MIMO) antenna is illustrated across four steps, i.e., A1 to A4. In the first step, the development of the UWB antenna is depicted. Then, the generation of the four stopbands is described gradually, and the proposed antenna configuration is shown in the last step.

3. FABRICATION AND MEASUREMENT

As shown in Fig. 5, the prototype antenna is fabricated and measured. The measured and simulated S_{11} for the X-band are presented in Fig. 6. The measured S_{11} of the proposed AVA is lower than -15 dB in the whole operating frequency band, indicating that the proposed AVA obtains good impedance-matching performances in X-band obviously. Good agreement is achieved between the simulated and measured results. However, at higher frequencies, fabrication issues, especially substrate cut, cause discrepancies between simulation and experiment. Notice that the measured max E field is not given, due to the limitation of the measurement facility.

Gain patterns for both E- and H-planes are depicted in Fig. 7. The co-polarization in both planes for measurement and experiment is plotted at 8, 9, 10, and 12 GHz. The proposed AVA has an end-fire characteristic over the operating frequency band. Meanwhile, the measured co-polarization radiation pattern of the X-band is symmetrical and in accord with simulated one.

TABLE 2. Comparison between the proposed antenna and previous models.

Ref.	Type	Size	Power capcacity	BW (GHz)	Efficiency
[24]	Vivaldi	45 mm × 40 mm ($1.46\lambda_m \times 1.3\lambda_m$)	NG	2.79–16.66	76.7%
[25]	Vivaldi	5 mm × 2.5 mm ($1.46\lambda_m \times 1.3\lambda_m$)	NG	58–62	$>96\%$
[26]	Vivaldi	85 mm × 110 mm ($3.4\lambda_m \times 4.4\lambda_m$)	NG	6–18	NG
[27]	Vivaldi	260 mm × 120 mm ($12.6\lambda_m \times 5.82\lambda_m$)	NG	2.8–15	NG
Pro.	**Vivaldi**	**13.2 mm×12.6 mm ($0.44\lambda_m \times 0.42\lambda_m$)**	**820 kW**	**8–12**	**$>91\%$**

λ_m is the wavelength referring to the center frequency of the operating band.

Moreover, the cross polarization is not illustrated in Fig. 7 for simplicity. Besides, it should be noted that discrepancies between the simulated and measured results may be caused by unexpected errors or tolerance in the fabrication and assembly, as well as the effect of the measurement environment.

Obviously, adding the circularly shaped loads and several elliptic slits etched into the tapered slot can cause a relatively distinct impact on unsteady radiation patterns, which is realized in several operating frequency bands. Table 2 compares the configuration of the conventional high-power antennas and the proposed antenna at X-band. It is evident that the proposed antenna obtains comprehensive performance in compact size, high power, low weight, gain, and efficiency. Therefore, when it comes to the demand of miniaturization, high-power designed antenna in X-band, the proposed AVA is still an attractive candidate in these fields and has great potential for the application in array design.

4. CONCLUSION

A miniaturized AVA, consisting of circularly shaped loads and some elliptic slits etched into the tapered slot can increase the max power capacity of the AVA and broaden the bandwidth for operating in X-band respectively, which has been designed and experimentally studied in this paper. As a result, the measured S_{11} of X-band is less than -15 dB, and antenna efficiency is higher than 91%, showing that the proposed AVA has great impedance characteristics. Moreover, the proposed AVA has the max power capacity of 820 KW and an especially size of $0.44\lambda_{\text{middle}} \times 0.42\lambda_{\text{middle}}$ (13.2 mm × 12.6 mm). The above superiorities make the proposed antenna suitable for high-power design and applied in X-band.

ACKNOWLEDGEMENT

The authors would thank the editors and anonymous reviewers for their efforts in evaluating our manuscript.

This work was supported by the National Natural Science Foundation of China Grant 62271407.

REFERENCES

[1] Zhao, L., Y. Wang, C. Liu, D. Song, C. Hu, C. Li, H. Zhao, and Z. Wang, "Compact circular-shaped MIMO antenna covers UWB bandwidth with four frequently-used band-notched characteristics for multi-scenario applications," *IEEE Access*, Vol. 12, 32 762–32 771, 2024.

[2] Zhu, H., G. Liu, L. Zhao, J. Xu, Y. Di, and H. Zhao, "Ultrawideband, dual-linearly polarized tightly coupled dipole array with composite wide-angle scanning superstrate," in *2023 IEEE International Symposium on Antennas and Propagation (ISAP)*, 1–2, Kuala Lumpur, Malaysia, Oct.–Nov. 2023.

[3] Zhao, L., H. Zhu, C. Ding, G. Liu, H. Zhao, J. Mou, and Y. J. Guo, "An ultrawideband dual-polarized tightly coupled dipole array (TCDA) with wide scanning range," *IEEE Antennas and Wireless Propagation Letters*, Vol. 23, No. 7, 1961–1965, 2023.

[4] Yang, M., H. Peng, K. Zheng, and G. Wei, "Spatial radiation field distribution of underwater VLF two-element antenna array," *IEEE Transactions on Antennas and Propagation*, Vol. 71, No. 1, 1164–1169, 2022.

[5] Huda, S., A. Saha, and A. Karmakar, "Ultra wideband (UWB) dielectric resonator antenna using fractal-inspired feeding mechanism," *International Journal of Communication Systems*, Vol. 36, No. 13, e5519, 2023.

[6] Agarwal, M., J. K. Dhanoa, and M. K. Khandelwal, "Two-port hexagon shaped MIMO microstrip antenna for UWB applications integrated with double stop bands for WiMax and WLAN," *AEU — International Journal of Electronics and Communications*, Vol. 138, 153885, 2021.

[7] Wang, S.-F. and Y.-Z. Xie, "Design and optimization of high-power UWB combined antenna based on Klopfenstein impedance taper," *IEEE Transactions on Antennas and Propagation*, Vol. 65, No. 12, 6960–6967, 2017.

[8] Yuan, C.-W., S.-R. Peng, T. Shu, Z.-Q. Li, and H. Wang, "Designs and experiments of a novel radial line slot antenna for high-power microwave application," *IEEE Transactions on Antennas and Propagation*, Vol. 61, No. 10, 4940–4946, 2013.

[9] Pottier, S. B., F. Hamm, D. Jousse, P. Sirot, F. T. Talom, and R. Vézinet, "High pulsed power compact antenna for high-power microwaves applications," *IEEE Transactions on Plasma Science*, Vol. 42, No. 6, 1515–1521, IEEE, 2014.

[10] Liang, Y., J. Zhang, Q. Liu, and X. Li, "High-power radial-line helical subarray for high-frequency applications," *IEEE Transactions on Antennas and Propagation*, Vol. 66, No. 8, 4034–4041, 2018.

[11] Ling, G. s. and C. W. Yuan, "Design of a Vlasov antenna with reflector," *International Journal of Electronics*, Vol. 91, No. 4, 253–258, 2004.

[12] Fazaelifar, M. and M. Fatorehchy, "Design, fabrication and test of parabolic cylinder reflector and horn for increasing the gain of Vlasov antenna," *Progress In Electromagnetics Research Letters*, Vol. 4, 191–203, 2008.

[13] Becker, E. C., S. D. Kovaleski, and J. M. Gahl, "Optimization of a compact conical horn antenna system for high power microwaves in the 4 to 6 GHz range," *IEEE Transactions on Dielectrics and Electrical Insulation*, Vol. 18, No. 4, 1066–1070,

2011.

[14] Zhao, L., Y. Wang, D. Song, C. Liu, C. Li, H. Zhao, and C. Hu, "Compact Vivaldi antenna application in high-power design at X-band," in *2024 18th European Conference on Antennas and Propagation (EUCAP)*, 1–3, Glasgow, United Kingdom, Mar. 2024.

[15] Zhao, L., C. Liu, C. Li, D. Song, Y. Wang, Y. Liang, H. Zhao, and C. Hu, "A novel helical antenna for high-power design in X-band," *AEU — International Journal of Electronics and Communications*, Vol. 168, 154725, 2023.

[16] Gibson, P. J., "The Vivaldi aerial," in *1979 9th European Microwave Conference*, 101–105, 1979.

[17] Gazit, E., "Improved design of the Vivaldi antenna," in *IEE Proceedings H (Microwaves, Antennas and Propagation)*, Vol. 135, No. 2, 89–92, 1988.

[18] Fei, P., Y.-C. Jiao, W. Hu, and F.-S. Zhang, "A miniaturized antipodal Vivaldi antenna with improved radiation characteristics," *IEEE Antennas and Wireless Propagation Letters*, Vol. 10, 127–130, 2011.

[19] Teni, G., N. Zhang, J. Qiu, and P. Zhang, "Research on a novel miniaturized antipodal Vivaldi antenna with improved radiation," *IEEE Antennas and Wireless Propagation Letters*, Vol. 12, 417–420, 2013.

[20] Natarajan, R., J. V. George, M. Kanagasabai, and A. K. Shrivastav, "A compact antipodal Vivaldi antenna for UWB applications," *IEEE Antennas and Wireless Propagation Letters*, Vol. 14, 1557–1560, 2015.

[21] Biswas, B., R. Ghatak, and D. R. Poddar, "A fern fractal leaf inspired wideband antipodal Vivaldi antenna for microwave imaging system," *IEEE Transactions on Antennas and Propagation*, Vol. 65, No. 11, 6126–6129, 2017.

[22] Mirbeik-Sabzevari, A., S. Li, E. Garay, H.-T. Nguyen, H. Wang, and N. Tavassolian, "W-band micromachined antipodal Vivaldi antenna using SIW and CPW structures," *IEEE Transactions on Antennas and Propagation*, Vol. 66, No. 11, 6352–6357, 2018.

[23] Shi, X., Y. Cao, Y. Hu, X. Luo, H. Yang, and L. H. Ye, "A high-gain antipodal vivaldi antenna with director and metamaterial at 1-28 GHz," *IEEE Antennas and Wireless Propagation Letters*, Vol. 20, No. 12, 2432–2436, 2021.

[24] Sasikala, S., K. Karthika, S. Arunkumar, K. Anusha, S. Adithya, and A. J. A. Al-Gburi, "Design and analysis of a low-profile tapered slot UWB Vivaldi antenna for breast cancer diagnosis," *Progress In Electromagnetics Research M*, Vol. 124, 43–51, 2024.

[25] Ibrahim, I. M., M. I. Ahmed, H. M. Abdelkader, A. J. A. Al-Gburi, and M. M. Elsherbini, "A miniaturized and high-gain antipodal Vivaldi antennas using directors," *Progress In Electromagnetics Research Letters*, Vol. 118, 2024.

[26] Sang, L., S. Wu, G. Liu, J. Wang, and W. Huang, "High-gain UWB Vivaldi antenna loaded with reconfigurable 3-D phase adjusting unit lens," *IEEE Antennas and Wireless Propagation Letters*, Vol. 19, No. 2, 322–326, 2019.

[27] Wang, Y.-W. and Z.-W. Yu, "A novel symmetric double-slot structure for antipodal Vivaldi antenna to lower cross-polarization level," *IEEE Transactions on Antennas and Propagation*, Vol. 65, No. 10, 5599–5604, 2017.